Effect of Fabrication Parameters on Three-Dimensional Nanostructures and Device Efficiency of Polymer Light-Emitting Diodes

Bang-Ying Yu,[†] Chia-Yi Liu,[†] Wei-Chun Lin,[†] Wei-Ben Wang,[§] I-Ming Lai,[§] Sun-Zen Chen,[⊥] Szu-Hsian Lee,[‡] Che-Hung Kuo,[‡] Wei-Lun Kao,[‡] Yun-Wen You,[†] Chi-Ping Liu,[†] Hsun-Yun Chang,[†] Jwo-Huei Jou,[§] and Jing-Jong Shyue[†,‡,*]

[†]Research Center for Applied Sciences, Academia Sinica, Taipei 115, Taiwan, [‡]Department of Materials Science and Engineering, National Taiwan University, Taipei 106, Taiwan, [§]Department of Materials Science and Engineering, National Tsing Hua University, Hsin-Chu 300, Taiwan, and [⊥]Center for Nanotechnology, Materials Science, and Microsystems, National Tsing Hua University, Hsin-Chu, Taiwan 300, Taiwan

ABSTRACT By using 10 kV C_{60}^+ and 200 V Ar^+ ion co-sputtering, a crater was created on the light-emitting layer of phosphorescent polymer light-emitting diodes, which consisted of a poly(9-vinyl carbazole) (PVK) host doped with a 24 wt % iridium(III)bis[(4,6-difluorophenyl)pyridinato-*N*,*C*^{2}] (FIrpic) guest. A force modulation microscope (FMM) was used to analyze the nanostructure at the flat slope near the edge of the crater. The three-dimensional distribution of PVK and FIrpic was determined based on the difference in their mechanical properties from FMM. It was found that significant phase separation occurred when the luminance layer was spin coated at 30 °C, and the phase-separated nanostructure provides a route for electron transportation using the guest-enriched phase. This does not generate excitons on the host, which would produce photons less effectively. On the other hand, a more homogeneous distribution of molecules was observed when the layer was spin coated at 60 °C. As a result, a 30% enhancement in device performance was observed.

KEYWORDS: cluster ion sputtering · force modulation microscopy · nanostructure · light-emitting diode · organic electronics

Since the discovery of conducting polymers, organic electronics have gained popularity because of their simple fabrication process and relatively low cost, as compared with silicon-based optoelectronic devices. In addition, the properties of organic materials can be easily tailored through the design of the molecular structure. As a result, organic electronics have evolved as a promising candidate for next-generation electronics. Currently, the most mature organic photonic devices are organic electroluminescent (OEL) and organic photovoltaic (OPV) devices.

It is known that the nanostructure of a material significantly affects the device properties. However, unlike inorganic semiconductors, which are usually crystalline, organic materials are mostly amorphous. As a result, it has been difficult to analyze the nanostructure inside organic electronics. In recent studies on the nanostructure of OPVs, such as the active layer of the P3HT:PCBM bulk heterojunction in polymer solar cells, the relationship between polymer morphology and device efficiency is reported.[1−3] To analyze polymer bulk heterojunctions, the surface morphology and vertical distribution of molecules in the polymer film are investigated by a variety of techniques, such as scanning probe microscopy (SPM)[4−8] and variable-angle spectroscopic ellipsometry (VASE),[9] respectively. However, these well-established techniques do not possess high resolution in three dimensions, so they cannot provide three-dimensional (3D) volume structures.

Recently, on the basis of transmission electron microscopy (TEM), electron tomography (ET) has been used to directly examine the 3D structure inside bulk heterojunctions.[2,10,11] However, because of the limitation in tilt angle, it is impossible to acquire complete information for 3D reconstruction. Therefore, the missing wedge in Fourier space causes artifacts in the resulting reconstructed structure.[12] Moreover, TEM-based techniques yield weak contrast in amorphous materials, making it difficult to obtain the 3D structure of amorphous organic electronics. In particular, OELs that have a high glass transition temperature are advantageous for highly efficient devices.[13,14] It is difficult to generate contrast of OELs using TEM because of their amorphous nature. As a result, while significant efforts are being directed at analyzing

*Address correspondence to shyue@gate.sinica.edu.tw.

Received for review November 11, 2009 and accepted April 21, 2010.

Published online April 28, 2010.
10.1021/nn901593c

the 3D nanostructure of OPVs, the structure inside OELs is currently understudied.

OELs have evolved as promising candidates for flat panel displays and solid-state lighting applications.[15−19] The Research Institute for Organic Electronics has predicted that OELs could occupy 25% of the lighting market and reduce 2.3% of CO_2 emissions by 2020. Over the past 10 years, phosphorescent materials have been especially apparent in OELs because of their ability to yield both singlet and triplet excitons, enabling nearly 100% internal quantum efficiency.[17,20−23] Therefore, to achieve high efficiency, OEL devices containing phosphorescent dopants are a more favorable choice. In a recent survey on the use of Ir-based dopants, such as iridium(III)bis[(4,6-difluorophenyl)pyridinato-*N*,C^2] picolinate (FIrpic), or ionic iridium complexes doped in a nonconjugated polymer host, like poly(9-vinyl carbazole) (PVK), high efficiency polymer light-emitting diodes (PLEDs) were reported as one type of phosphorescent OEL.[24,25]

In PLEDs, the amorphous and oriented phase segregation of the polymer is highly sensitive to the fabrication process.[26,27] Additional phase separation in polymer films is often found upon mixing with small molecules that have significantly different chemical structures. This phase separation is crucial to device efficiency.[28] Therefore, investigating and understanding the relationship between fabrication parameters, nanostructures in the polymer film, and device performance is valuable to polymeric organic electronics.

On the basis of ion-beam depth profiling, the vertical nanostructure of organic opto-electronic devices has been studied with X-ray photoelectron spectrometry (XPS)[29−32] and time-of-flight secondary ion mass spectrometry (ToF-SIMS).[31] It was found that, although cluster ion sputtering significantly altered the outermost surface of inorganic materials,[33] it caused insignificant damage to the organic surface. This is because of the shallower damage range[34] and enhanced sputtering rate.[35] XPS and ToF-SIMS possess limited lateral resolution, allowing only the vertical structure to be probed. Thus, ion-beam depth profiling has been combined with scanning techniques, such as scanning electrical potential microscopy (SEPM)[36] and scanning ToF-SIMS,[37] to produce 3D volumetric images inside organic materials. Compared with ET, which yields similar 3D images, these techniques are independent of the crystallinity but only detect the nature of the chemical species. Thus, they are more general for analyzing organic materials.

While noteworthy efforts are made on studying bulk heterojunctions, investigations into the nanostructure inside PLEDs have been superficial. Furthermore, the relationship between fabrication process parameters, nanostructure, and device performance is unclear.[28,38] In this work, a C_{60}^+ cluster ion beam was used to sputter surface materials away, generating a crater in the specimen. Force modulation microscopy (FMM)[39] was then used to examine the edge of the crater. Because the slope at the edge was flat, the resulting image yielded the 3D nanostructure of PLEDs that were fabricated with different parameters. FMM data obtained in this work provide a contrast that arises from the difference in elastic properties of polymers and small molecules that have significantly different chemical structures. This contrast is an additional physical dimension and can be related to the degree of phase separation. Using this imaging technique to study the nanostructure of light-emitting layers fabricated at different temperature, it was found that, by suppressing the nanoscale phase separation, the efficiency of the device was enhanced. This difference in efficiency was attributed to better carrier trapping inside the emissive layer of the device.

RESULTS AND DISCUSSION

It has been reported that C_{60}^+ ion sputtering could alter the mechanical properties of a remaining surface, especially with a high energy beam.[40] Although it has been shown that a 10 kV beam does not alter the elastic modulus of PMMA significantly,[40] the possibility of ion-beam-induced FMM contrast needs to be ruled out. Figure 1 shows the FMM image of a reference PVK film before and after ion-beam sputtering. The FMM amplitude line profile of pristine PVK (overlay on Figure 1a) shows an amplitude range of about 60 mV. This could be attributed to the natural folding of the PVK polymer. The topographical image (Figure 1b) shows the aggregation of the polymer. Intensity correlation analysis (Figure 1c) was carried out on the FMM and topographical image. The intensity correlation quotient (ICQ) of 0.033 indicated weak or no correlation between these two images. In other words, the different features revealed in the FMM amplitude and morphology clearly indicate that the topographic information is decoupled from the mechanical properties.

After ion-beam sputtering, granular features were observed on the surface (Figure 1e) and were consistent with the usually observed sputtering-induced morphology.[34] As a result, the FMM contrast (Figure 1d) became less continuous, indicating that the sputtering procedure slightly altered the mechanical properties of the sample. This shows up as approximately 20 mV of contrast in the image. Nevertheless, an amplitude range of about 50 mV in FMM was still clearly observed. Such a difference in contrast can be analyzed with the histogram of FMM images (Figure 2). It is clear that, after sputtering, the contrast range decreased and the contrast arose from the difference in mechanical properties weakened. This result indicates that the FMM image acquired after sputtering might underestimate the phase separation by around 10 mV. As a result, if the original difference in mechanical properties is too small, features could be smeared and would not be observable.

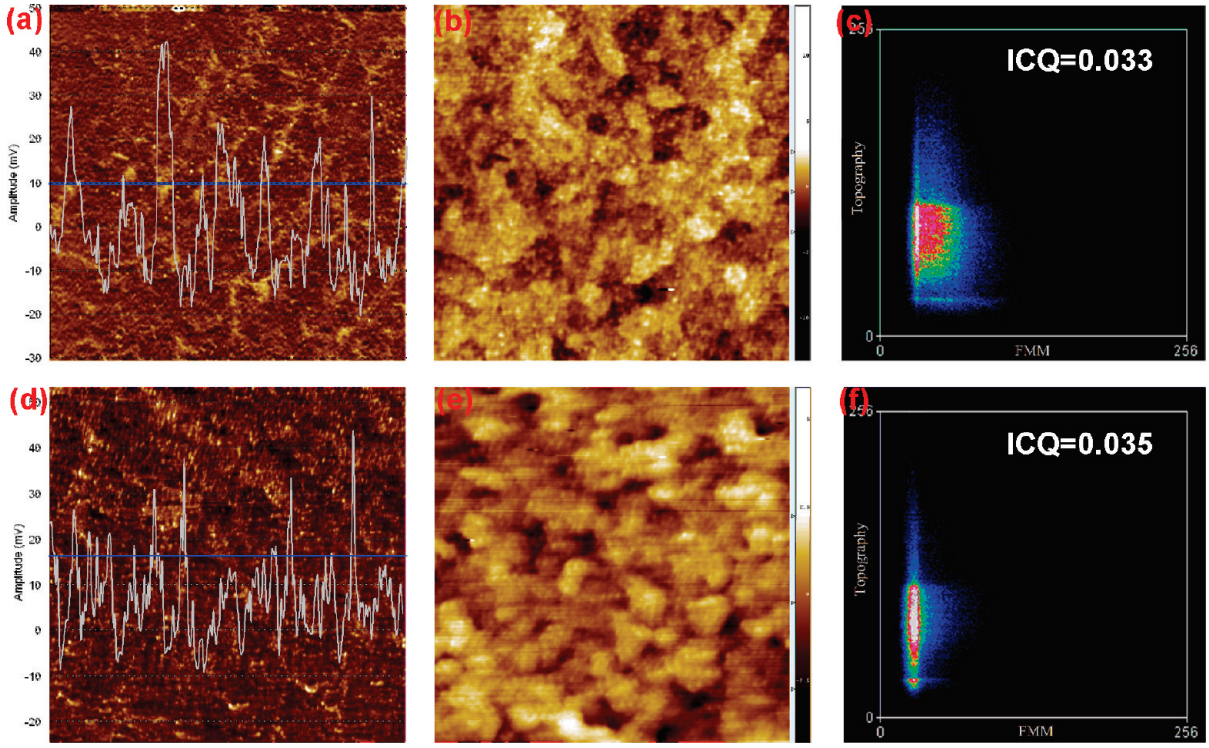

Figure 1. (a,d) FMM amplitude image of a reference PVK film before and after ion-beam sputtering, respectively. A brightness (FMM amplitude) line profile obtained at the image center (solid line) is overlaid on the image. (b,e) Associated surface topography. The field of view is 5 μm × 5 μm. (c,f) Frequency scattered plot between FMM amplitude and topography.

Although the surface morphology does not contain real information about the specimen, it is clear that, by comparing the images acquired before and after sputtering, the FMM contrast observed after sputtering can still reveal the nanostructure inside the specimen.

By using cluster ion sputtering, a crater is created on the specimen (Scheme 1). During sputtering, XPS was used to monitor the progress. The appearance of a S 2p signal indicated that the light-emitting layer was through and the bottom PEDOT:PSS exposed. Such craters are known to have a rather flat slope near the edge. In other words, for the FMM image obtained along the edge of the crater (ROI in Scheme 1), the *x*-axis of the image contains information from both *x*- and *z*-axes of the specimen.[36] Figures 3 and 4 show the FMM image obtained on the slope of PVK:FIrpic blends that were spin coated at 30 and 60 °C, respectively. The contrast range (Figure 2) of 260 and 186 mV for Figures 3 and 4, respectively, was well above the contrast level obtained on the referencing PVK film (60 mV). Thus, the observed feature could not be simply attributed to PVK folding. The different features inside films coated at different temperatures also suggest that the observed structure was not simply induced by sputtering. Furthermore, the similarity of the structures observed at different depths, upon being exposed to different ion-beam fluences, indicates that sputtering did not significantly alter the nanostructure. It is noted that the image was stitched from multiple 5 μm × 5 μm images, and vertical dark contrast is obvious near the stitching region in Figure 4. This artifact arose from the fact that the image was overscanned to aid in stitching. As a result, near the stitched area, the specimen was scanned twice with FMM, and the mechanical properties were slightly altered by the first

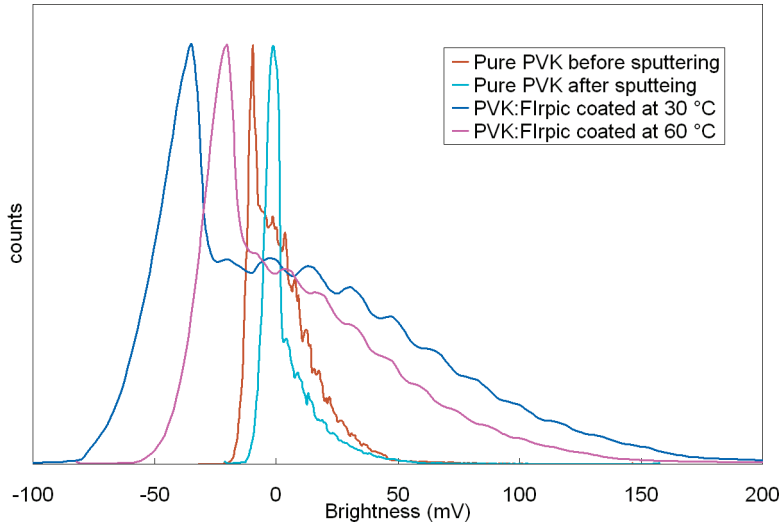

Figure 2. Histograms of FMM images acquired in this work.

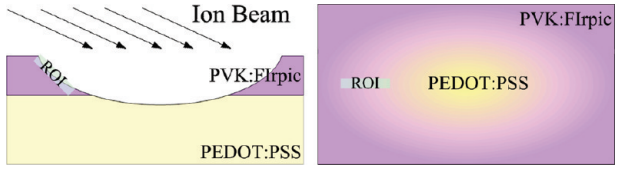

Scheme 1. Schematic drawing of the creation of a crater with an ion beam (not drawn to scale). (a) Side view and (b) top view of the crater. The ROI (region of interest) indicates the FMM imaging location.

scan. Thus, different contrast levels were observed near the stitch. This stitch is not clearly observable in Figure 3 because the contrast range was much larger than the artifact.

Using the force curve obtained with an atomic force microscope, the spring constants of polymeric PVK and molecular FIrpic were determined to be 28.8 and 255 nN/μm, respectively. Because FIrpic is stiffer than PVK and transmits the oscillation directly to the cantilever, while compliant PVK absorbs the oscillation, the oscillation amplitude of the tip was larger at the FIrpic-enriched region. In other words, the features shown in the resulting FMM images indicate the distribution of PVK (dark) and FIrpic (bright). In addition, the magnitude of the contrast indicates the degree of phase separation.

For PVK:FIrpic blends that were spin coated at 30 °C, the FMM image (Figure 3) clearly shows features that consist of an approximately 200 nm wide PVK-enriched region (dark contrast) and an approximately 100 nm wide FIrpic-enriched region (bright contrast). The histogram (Figure 2) revealed a narrow and broad distribution of the FMM intensity at dark and bright contrast area, respectively. This observation revealed uniform mechanical properties in the PVK-enriched region that in turn suggest a uniform molecular distribution in this region. On the other hand, the phase-segregated FIrpic-enriched region has a non-uniform chemical composition that could be attributed to the diffusion of the FIrpic molecule toward this region. The FIrpic-enriched region formed a continuous network through the thickness. In addition, the contrast range of 260 mV indicates that significant phase separation occurred in the blend. On the other hand, the PVK:FIrpic blend that was spin coated at 60 °C showed a weak contrast in the FMM image (Figure 4). The contrast range of the image was 186 mV, which is smaller than that coated at 30 °C. Furthermore, through the analysis of the histogram (Figure 2), it is clear that the areal fraction of brighter contrast is lower than that coated at 30 °C. This smaller contrast range and contrast difference indicates that the mechanical properties of this sample were more uniform; hence, the distribution of molecules was more uniform. In addition, the scattered

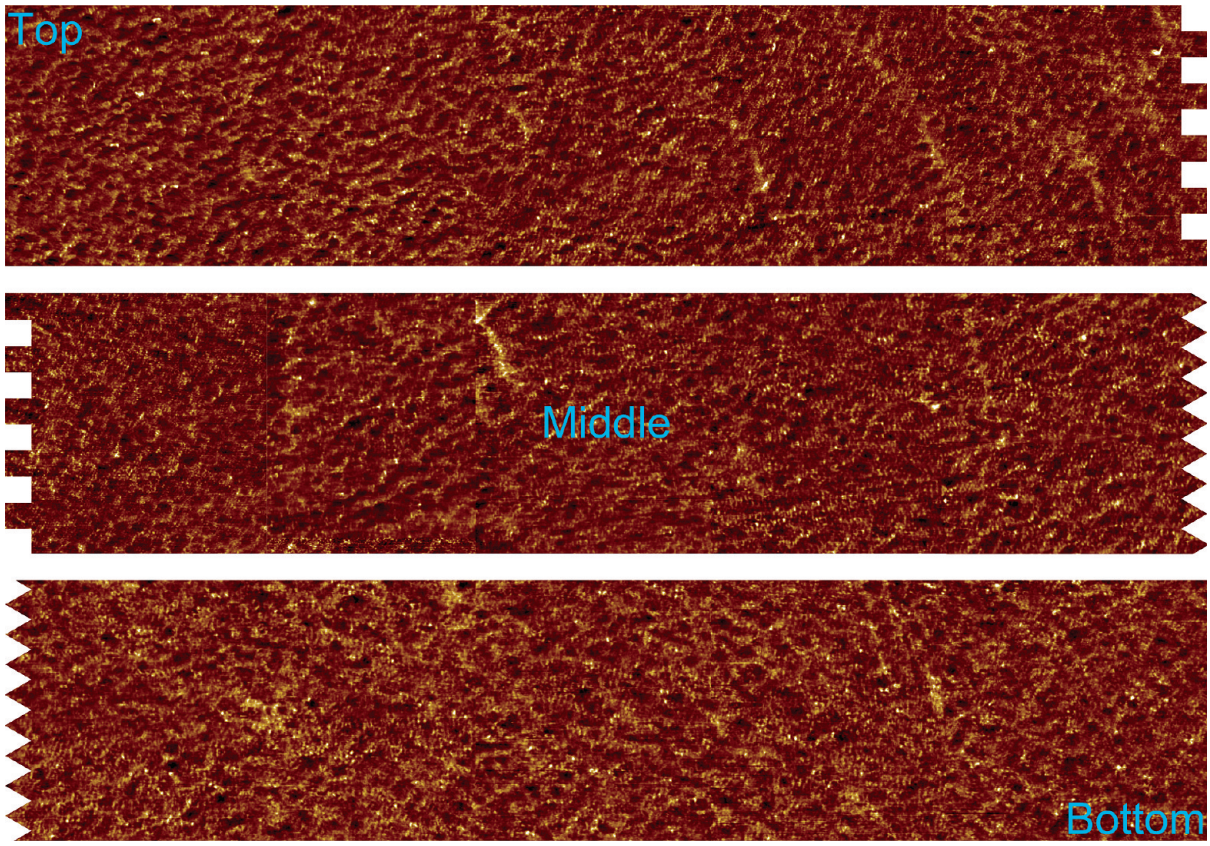

Figure 3. FMM amplitude image at the edge of a crater that was created by sputtering on a PVK:FIrpic blend spin that was coated at 30 °C. The contrast range was 260 mV, and the overall image size, after stitching images in each row, was 5 μm × 68 μm. This range reflects the structure at different depths of the film.

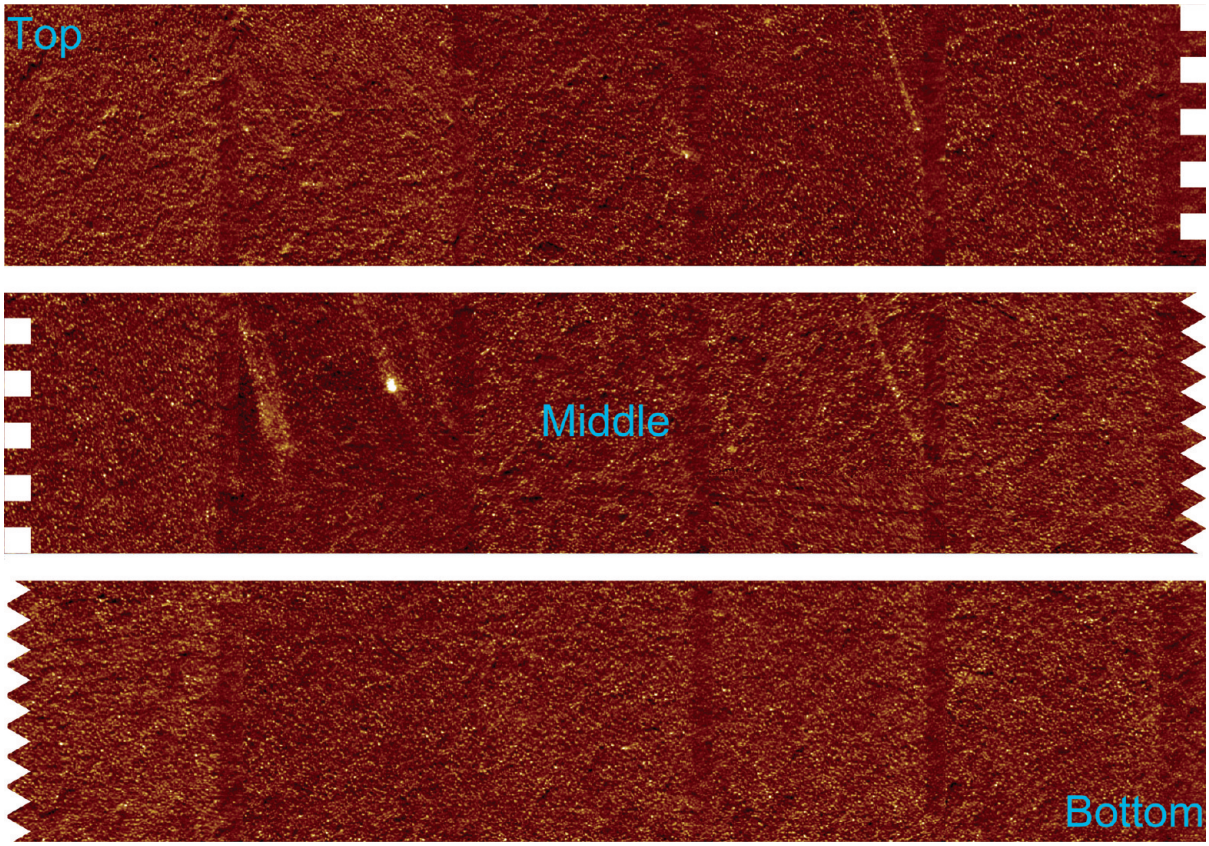

Figure 4. FMM amplitude image at the edge of a crater, which was created by sputtering on a PVK:FIrpic blend that was spin coated at 60 °C. The contrast range was 186 mV, and the overall image size after stitching images in each row was 5 μm × 68 μm. This range reflects the structure at different depths of the film.

bright spots of around 60 nm in diameter indicate a small aggregation of FIrpic. These aggregates did not form a continuous phase, compared with samples that were spin coated at 30 °C. Furthermore, the FIrpic-deficient phase (dark contrast) was continuous.

In the extensive research that has been performed on polymer bulk heterojunctions, it is known that post-annealing,[9] solvent-assisted annealing,[3] and slow drying[5] induce the phase separation. In this work, when coated at 60 °C, the solvent dried faster than when coated at 30 °C. In addition, the temperature was significantly lower than for post-annealing, and molecules did not have enough energy to diffuse. As a result, the PVK:FIrpic blend that was spin coated at 60 °C possessed a more uniform molecular distribution, while that coated at 30 °C yielded significant phase separation.

Nanostructural differences affect the device properties significantly. Using a device structure of ITO/PEDOT:PSS/PVK:FIrpic/TPBi/LiF/Al, the properties of devices fabricated with different processing temperatures of

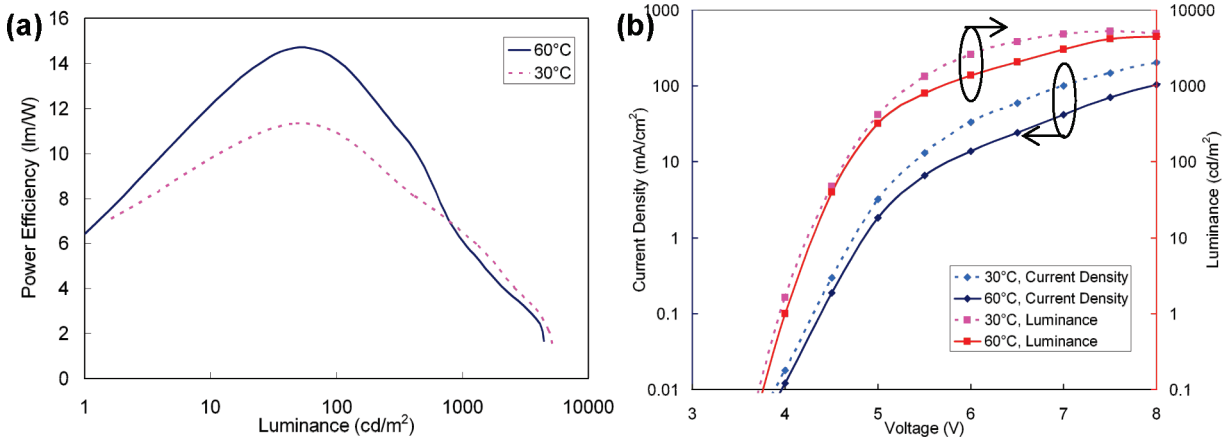

Figure 5. (a) Power efficiency and (b) electrical properties of devices containing luminance layers that were spin coated at 30 °C (broken lines) and 60 °C (solid lines).

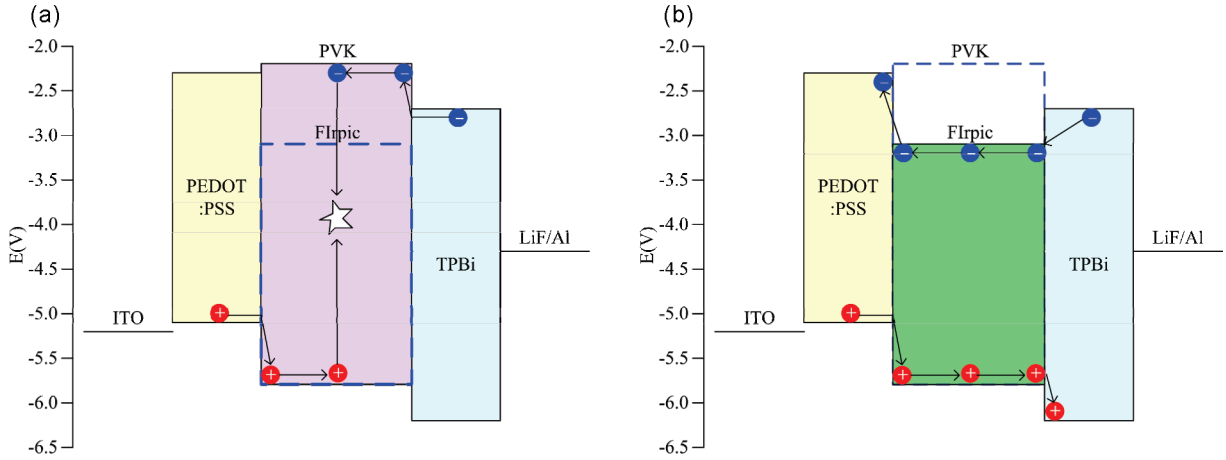

Figure 6. Theoretical energy diagram and path of charge carrier in (a) PVK-enriched and (b) FIrpic-enriched phases.

light-emitting layers were assessed, as shown in Figure 5. It is evident that the power efficiency was enhanced dramatically upon an increase in processing temperature of the PVK:FIrpic blend. These devices were identical in terms of the device architecture and thickness of each layer. Furthermore, the identical electroluminance properties and CIE coordinates (0.18, 0.33) indicated that the fabrication parameter did not affect the molecular energetics. Therefore, the difference in efficiency must have been due to differences in the nanostructure of PVK:FIrpic.

Considering the theoretical energy diagram of the device (Figure 6), it is known that charge carriers must be trapped on a PVK host and that they generate excitons on PVK upon recombination. After an energy transfer from PVK to FIrpic, photons are generated. For devices fabricated at a lower temperature (30 °C), significant phase separations were observed. These devices can be described as FIrpic-enriched networks in PVK-enriched matrices (Figure 3). In the PVK-enriched phase, the charge carriers could be trapped on PVK (Figure 6a), generating photons effectively. On the other hand, in the FIrpic-enriched phase, it was easier for an electron to enter the FIrpic that had a higher concentration and no energy barrier. In addition, because the FIrpic-enriched phase formed a continuous network between electron-transporting (TPBi) and hole-transporting (PEDOT:PSS) layers, electrons could easily move through the luminance layer *via* this phase (Figure 6b). Although excitons also formed on the FIrpic guest, these excitons tended to quench with each other, causing a color shift[41] and lowering its efficiency.[42] In other words, because these electrons were not trapped on PVK, it could not generate excitons in the host and hence could not transfer energy from host to guest. As a result, the photon generation was less efficient. On the other hand, for a more homogeneously mixed PVK:FIrpic blend that was spin coated at 60 °C, the continuous PVK-enriched phase forced the carrier to be trapped on the host. Thus, excitons generated in the PVK host could easily diffuse to the FIrpic-enriched phase that was scattered on the nanometer scale (Figure 4) and generate photons efficiently. As a result, the luminance layer that was spin coated at 60 °C produced 30% better efficiency.

The electrical properties (Figure 5b) also reflect the effect of nanoscale phase separation. For the luminance layer coated at 30 °C, the current density was higher than that coated at 60 °C. This is because the FIrpic-enriched continuous phase provided a route for electron transportation and trapped electrons less effectively. In terms of driving voltage (the voltage required to reach 10 cd/m^2), the device prepared at 30 °C was lower (4.1 V) than that at 60 °C (4.2 V). This is because it was easier for electrons to move into the phase-separated luminance layer through the FIrpic-enriched phase.

CONCLUSION

On the basis of cluster ion sputtering, a crater was created on the emissive layer of a polymeric light-emitting diode, which consisted of a FIrpic guest that was doped in a PVK host. By analyzing the mechanical properties, using force modulation microscopy at the edge of the crater, 3D molecular distributions of FIrpic and PVK were obtained. It was found that significant phase separation occurred when the PVK:FIrpic blend was coated at 30 °C. In addition, the FIrpic-enriched phase formed a continuous 3D network inside the luminance layer. On the other hand, a PVK:FIrpic blend that was coated at 60 °C was more homogeneous, due to fast drying. The approximately 60 nm FIrpic-enriched phase was scattered in the continuous PVK-enriched phase. The continuous FIrpic-enriched nanostructures formed at 30 °C provided a route for electrons to pass through the luminance layer without efficient energy transfer. In contrast, the nanostructures formed from the 60 °C process could trap charge carriers on PVK, allowing excitons to diffuse to the scattered FIrpic guest. As a result, a 30% enhancement in device efficiency was observed.

METHODS

Fabrication of Light-Emitting Films: Polymeric blue emissive layers (ELs), containing 24 wt % FIrpic guest doped in PVK host, were prepared by spin coating the corresponding solution on a poly(ethylene dioxythiophene):polystyrenesulfonate (PEDOT:PSS, 46 nm) modified ITO (150 nm) substrate under nitrogen atmosphere. The host and guest materials were dissolved in toluene at 75 °C with stirring. The well-mixed solutions were cooled to room temperature (30 °C) or heated again to 60 °C before spin coating at 5000 rpm. The PVK:FIrpic layer was 23 nm thick. The pure PVK film, which served as a reference, was spin coated on a PEDOT:PSS layer at room temperature.

Device Fabrication and Characterization: On the light-emitting films, a 2,2′,2′′-(1,3,5-benzinetriyl)tris(1-phenyl-1*H*-benzimidazole) (TPBi) electron-transporting layer (32 nm) was thermoevaporated. An additional electron injection layer (0.7 nm) of LiF and Al cathode (150 nm) was evaporated onto the TPBi. The luminescence area was 5 mm × 5 mm. The electrical properties of the prepared device were measured with a 2400 Sourcemeter (Keithley, Cleveland, OH), and the luminance was measured with a CS-100A colorimeter (Konica Minolta Sensing Inc., Osaka, Japan). Measurements on these face-emitting devices were taken in the ambient environment, without encapsulation.

Ion Sputtering: Cluster ion sputtering was carried out with a PHI 5000 VersaProbe Scanning ESCA Microprobe (ULVAC-PHI, Chigasaki, Japan) system. A charge neutralizer (30 V flooding electron beam) was used to compensate for the charge buildup effect during sputtering. The Ar^+ ion source (FIG-5CE), which was set at a fixed incident angle of 45°, was operated at 0.2 kV and 300 nA using a floating voltage of 500 V and a spot size of approximately 200 μm. A Wien-filtered C_{60}^+ ion source (IOG C60-10, Ionoptika, Chandler's Ford, UK) was operated at 10 nA and 10 kV (spot size of about 600 μm) at a fixed incident angle of 70° (from the normal to the surface of analysis). The beam current was measured by the sample current on a Au foil and was controlled by the strength of the condenser lens. The ion beams were rastered over an area of 2 mm × 2 mm. The low-energy Ar^+ ion beam and high-energy C_{60}^+ ion beam were used concurrently to effectively remove the surface with minimal damage.[30]

FMM Measurements: Experiments were performed with a Veeco Innova (Woodbury, NY) atomic force microscope, using a 75 kHz cantilever in the contact mode. The probe cartridge was oscillated at the resonance frequency of the probe, which was about 13 kHz. Because the oscillation frequency was much higher than the height feedback loop, the DC component of the deflection signal was used to maintain constant tip-to-sample spacing for determining and decoupling sample topography. The AC component of the deflection, in terms of the amplitude and phase, was measured by a dedicated lock-in circuit, yielding the FMM amplitude and FMM phase image, respectively.

Acknowledgment. The authors acknowledge sponsorships by the Academia Sinica, Ministry of Economic Affairs, and Taiwan National Science Council through Grant Nos. 98-2113-M-001-012-MY2 and 98-2120-M-002-005.

REFERENCES AND NOTES

1. Zhang, F. L.; Jespersen, K. G.; Bjorstrom, C.; Svensson, M.; Andersson, M. R.; Sundstrom, V.; Magnusson, K.; Moons, E.; Yartsev, A.; Inganas, O. Influence of Solvent Mixing on the Morphology and Performance of Solar Cells Based on Polyfluorene Copolymer/Fullerene Blends. *Adv. Funct. Mater.* **2006**, *16*, 667–674.
2. Yang, X.; Loos, J. Toward High-Performance Polymer Solar Cells: The Importance of Morphology Control. *Macromolecules* **2007**, *40*, 1353–1362.
3. van Bavel, S. S.; Sourty, E.; With, G. D.; Loos, J. Three-Dimensional Nanoscale Organization of Bulk Heterojunction Polymer Solar Cells. *Nano Lett.* **2009**, *9*, 507–513.
4. Bull, T. A.; Pingree, L. S. C.; Jenekhe, S. A.; Ginger, D. S.; Luscombe, C. K. The Role of Mesoscopic PCBM Crystallites in Solvent Vapor Annealed Copolymer Solar Cells. *ACS Nano* **2009**, *3*, 627–636.
5. Xu, Z.; Chen, L. M.; Yang, G. W.; Huang, C. H.; Hou, J. H.; Wu, Y.; Li, G.; Hsu, C. S.; Yang, Y. Vertical Phase Separation in Poly(3-hexylthiophene): Fullerene Derivative Blends and Its Advantage for Inverted Structure Solar Cells. *Adv. Funct. Mater.* **2009**, *19*, 227–234.
6. Palermo, V.; Ridolfi, G.; Talarico, A. M.; Favaretto, L.; Barbarella, G.; Camaioni, N.; Samori, P. A Kelvin Probe Force Microscopy Study of the Photogeneration of Surface Charges in All-Thiophene Photovoltaic Blends. *Adv. Funct. Mater.* **2007**, *17*, 472–478.
7. Hoppe, H.; Glatzel, T.; Niggemann, M.; Hinsch, A.; Lux-Steiner, M. C.; Sariciftci, N. S. Kelvin Probe Force Microscopy Study on Conjugated Polymer/Fullerene Bulk Heterojunction Organic Solar Cells. *Nano Lett.* **2005**, *5*, 269–274.
8. Chiesa, M.; Burgi, L.; Kim, J. S.; Shikler, R.; Friend, R. H.; Sirringhaus, H. Correlation between Surface Photovoltage and Blend Morphology in Polyfluorene-Based Photodiodes. *Nano Lett.* **2005**, *5*, 559–563.
9. Campoy-Quiles, M.; Ferenczi, T.; Agostinelli, T.; Etchegoin, P. G.; Kim, Y.; Anthopoulos, T. D.; Stavrinou, P. N.; Bradley, D. D. C.; Nelson, J. Morphology Evolution *via* Self-Organization and Lateral and Vertical Diffusion in Polymer: Fullerene Solar Cell Blends. *Nat. Mater.* **2008**, *7*, 158–164.
10. Andersson, B. V.; Herland, A.; Masich, S.; Ingans, O. Imaging of the 3D Nanostructure of a Polymer Solar Cell by Electron Tomography. *Nano Lett.* **2009**, *9*, 853–855.
11. Moon, J. S.; Lee, J. K.; Cho, S.; Byun, J.; Heeger, A. J. "Columnlike" Structure of the Cross-Sectional Morphology of Bulk Heterojunction Materials. *Nano Lett.* **2009**, *9*, 230–234.
12. Arslan, I.; Tong, J. R.; Midgley, P. A. Reducing the Missing Wedge: High-Resolution Dual Axis Tomography of Inorganic Materials. *Ultramicroscopy* **2006**, *106*, 994–1000.
13. Shirota, Y. Organic Materials for Electronic and Optoelectronic Devices. *Mater. Chem.* **2000**, *10*, 1–25.
14. Chan, L. H.; Lee, R. H.; Hsieh, C. F.; Yeh, H. C.; Chen, C. T. Optimization of High-Performance Blue Organic Light-Emitting Diodes Containing Tetraphenylsilane Molecular Glass Materials. *J. Am. Chem. Soc.* **2002**, *124*, 6469–6479.
15. Kido, J.; Kimura, M.; Nagai, K. Multilayer White Light-Emitting Organic Electroluminescent Device. *Science* **1995**, *267*, 1332–1334.
16. Duggal, R.; Shiang, J. J.; Heller, C. M.; Foust, D. F. Organic Light-Emitting Devices for Illumination Quality White Light. *Appl. Phys. Lett.* **2002**, *80*, 3470.
17. Forrest, S. R. *Org. Electron.* **2003**, *4*, 45.
18. D'Andrade, W.; Forrest, S. R. White Organic Light-Emitting Devices for Solid-State Lighting. *Adv. Mater.* **2004**, *16*, 1585–1595.
19. Burn, P. L.; Lo, S. C.; Samuel, I. D. W. The Development of Light-Emitting Dendrimers for Displays. *Adv. Mater.* **2007**, *19*, 1675–1688.
20. Adachi, C.; Baldo, M. A.; Forrest, S. R. High-Efficiency Organic Electrophosphorescent Devices with Tris(2-phenylpyridine)iridium Doped into Electron-Transporting Materials. *Appl. Phys. Lett.* **2000**, *77*, 904.
21. Baldo, M. A.; O'Brien, D. F.; You, Y.; Shoustikov, A.; Sibley, S.; Thompson, M. E.; Forrest, S. R. Highly Efficient Phosphorescent Emission from Organic Electroluminescent Devices. *Nature* **1998**, *395*, 151–154.
22. Duan, J. P.; Sun, P. P.; Cheng, C. H. New Iridium Complexes as Highly Efficient Orange-Red Emitters in Organic Light-Emitting Diodes. *Adv. Mater.* **2003**, *15*, 224–228.
23. Kawamura, Y.; Goushi, K.; Brooks, J.; Brown, J. J.; Sasabe, H.; Adachi, C. 100% Phosphorescence Quantum Efficiency of Ir(III) Complexes in Organic Semiconductor Films. *Appl. Phys. Lett.* **2005**, *86*, 071104.
24. Mathai, M. K.; Choong, V. E.; Choulis, S. A.; Krummacher, B.; So, F. Highly Efficient Solution Processed Blue Organic Electrophosphorescence with 14 lm/W Luminous Efficacy. *Appl. Phys. Lett.* **2006**, *88*, 243512.
25. He, L.; Duan, L.; Qiao, J.; Zhang, D.; Dong, G.; Wang, L.; Qiu,

Y. Efficient Solution-Processed Electrophosphorescent Devices Using Ionic Iridium Complexes as the Dopants. *Org. Electron.* **2009**, *10*, 152–157.
26. Yang, C. Y.; Hide, F.; Diaz-Garcia, M. A.; Heeger, A. J.; Cao, Y. Microstructure of Thin Films of Photoluminescent Semiconducting Polymers. *Polymer* **1998**, *39*, 2299–2304.
27. Kim, J.; Lee, J.; Han, C. W.; Lee, N. Y.; Chung, I. J. Effect of Thermal Annealing on the Lifetime of Polymer Light-Emitting Diodes. *Appl. Phys. Lett.* **2003**, *82*, 4238–4240.
28. Yimsiri, P.; Mackley, M. R. Microstructure and Device Performance of Thin Film Light Emitting Polymers. *Thin Solid Films* **2007**, *515*, 3787–3796.
29. Chen, Y.-Y.; Yu, B.-Y.; Wang, W.-B.; Hsu, M.-F.; Lin, W.-C.; Lin, Y.-C.; Jou, J.-H.; Shyue, J.-J. XPS Depth Profiling of Organic Thin Films Using C_{60} Sputtering. *Anal. Chem.* **2008**, *80*, 501–505.
30. Yu, B.-Y.; Chen, Y.-Y.; Wang, W.-B.; Hsu, M.-F.; Tsai, S.-P.; Lin, W.-C.; Lin, Y.-C.; Jou, J.-H.; Chu, C.-W.; Shyue, J.-J. Depth Profiling of Organic Films with X-ray Photoelectron Spectroscopy Using C_{60}^+ and Ar^+ Co-Sputtering. *Anal. Chem.* **2008**, *80*, 3412–3415.
31. Lin, W.-C.; Lin, Y.-C.; Wang, W.-B.; Yu, B.-Y.; Iida, S.-i.; Tozu, M.; Hsu, M.-F.; Jou, J.-H.; Shyue, J.-J. Effect of Fabrication Process on the Microstructure and the Efficiency of Organic Light Emitting Diode. *Org. Electron.* **2009**, *10*, 459–464.
32. Lin, W.-C.; Wang, W.-B.; Lin, Y.-C.; Yu, B.-Y.; Chen, Y.-Y.; Hsu, M.-F.; Jou, J.-H.; Shyue, J.-J. Electron Migration of Small Molecules during the Degradation of Organic Light-Emitting Diodes. *Org. Electron.* **2009**, *10*, 581–586.
33. Lin, Y.-C.; Chen, Y.-Y.; Yu, B.-Y.; Lin, W.-C.; Kuo, C.-H.; Shyue, J.-J. Sputter-Induced Chemical Transformation in Oxoanions by Combination of C_{60}^+ and Ar^+ Ion Beams Analyzed with X-ray Photoelectron Spectrometry. *Analyst* **2009**, *134*, 945–951.
34. Yu, B.-Y.; Chen, Y.-Y.; Lin, W.-C.; Lin, Y.-C.; Shyue, J.-J. Sputter Damage in Si (001) Surface by Combination of C_{60}^+ and Ar^+ Ion Beams. *Appl. Surf. Sci.* **2008**, *255*, 2490–2493.
35. Cheng, J.; Wucher, A.; Winograd, N. Molecular Depth Profiling with Cluster Ion Beams. *J. Phys. Chem. B* **2006**, *110*, 8329–8336.
36. Yu, B.-Y.; Lin, W.-C.; Huang, J.-H.; Chu, C.-W.; Lin, Y.-C.; Kuo, C.-H.; Lee, S.-H.; Wong, K.-T.; Ho, K.-C.; Shyue, J.-J. Three-Dimensional Nanoscale Imaging of Polymer Bulk-Heterojunction by Scanning Electrical Potential Microscopy and C_{60}^+ Cluster Ion Slicing. *Anal. Chem.* **2009**, *81*, 8936–8941.
37. Yu, B.-Y.; Lin, W.-C.; Wang, W.-B.; Iida, S.-i.; Chen, S.-Z.; Liu, C.-Y.; Kuo, C.-H.; Lee, S.-H.; Kao, W.-L.; Yen, G.-J.; *et al.* Effect of Fabrication Parameters on Three-Dimensional Nanostructures of Bulk-Heterojunctions Imaged by High-Resolution Scanning ToF-SIMS. *ACS Nano* **2009**, *4*, 833–840.
38. Ramos, M. M. D.; Barbosa, H. M. C. How Can the Nanostructure Affect the Charge Transport in PLED? *Eur. Phys. J. Appl. Phys.* **2009**, *46*, 12509.
39. Troyon, M.; Wang, Z.; Pastre, D.; Lei, H. N.; Hazotte, A. Force Modulation Microscopy for the Study of Stiff Materials. *Nanotechnology* **1997**, *8*, 163–171.
40. Fisher, G. L.; Dickinson, M.; Bryan, S. R.; Moulder, J. C_{60} Sputtering of Organics: A Study using TOF-SIMS, XPS and Nanoindentation. *Appl. Surf. Sci.* **2008**, *255*, 819–823.
41. Jou, J. H.; Wang, C. J.; Lin, Y. P.; Chung, Y. C.; Chiang, P. H.; Wu, M. H.; Wang, C. P.; Lai, C. L.; Chang, C. Color-Stable, Efficient Fluorescent Pure-White Organic Light-Emitting Diodes with Device Architecture Preventing Excessive Exciton Formation on Guest. *Appl. Phys. Lett.* **2008**, *92*, 223504.
42. Jou, J. H.; Hsu, M. F.; Wang, W. B.; Chin, C. L.; Chung, Y. C.; Chen, C. T.; Shyue, J. J.; Shen, S. M.; Wu, M. H.; Chang, W. C.; *et al.* Solution-Processable, High-Molecule-Based Trifluoromethyl−Iridium Complex for Extraordinarily High Efficiency Blue-Green Organic Light-Emitting Diode. *Chem. Mater.* **2009**, *21*, 2565–2567.